Aalborg Universitet

Statistical Method of Estimating Semiconductor Switching Transition Time enabling Condition Monitoring of Megawatt Converters

Rannestad, Bjørn; Munk-Nielsen, Stig; Gadgaard, Kristian; Uhrenfeldt, Christian

Statistical Method of Estimating Semiconductor Switching Transition Time enabling Condition Monitoring of Mega Watt Converters

Bjørn Rannestad, Stig Munk-Nielsen, Kristian Gadgaard, and Christian Uhrenfeldt

Abstract—Detection of Insulated Gate Bipolar Transistor (IGBT) switching transition time (t_{tr}) is a promising Temperature Sensitive Electrical Parameter (TSEP) for condition monitoring of IGBT power modules in converters for wind turbines. The accuracy required on t_{tr} detection is in nano seconds, which typically requires precision timing circuitry, or Analog to Digital Conversion (ADC) rates in hundreds of Mega Samples Per Second (MSPS). A method on calculating the statistically estimated switching transition time ($\hat{t}_{tr}$) is proposed in this paper. During multiple switching transitions of an IGBT, the IGBT collector-emitter voltage (vce) may be sampled with sample rates in sub MSPS rates, yet with statistical accuracy on estimated $\hat{t}_{tr}$ in nano seconds. A stand alone Converter Monitoring Unit (CMU) which samples vce and IGBT current (i_c), was mounted in the converter of a multi Mega Watt (MW) field test wind turbine. The proposed method is validated by testing it on field data from the CMU and by testing it on synthetically generated data. The proposed method is an enabler for low-cost monitoring of converters for wind turbine field applications.

Index Terms—Insulated gate bipolar transistors, Monitoring, Sampling Methods

NOMENCLATURE

di_c/dt	Time derivative of semiconductor current
dv_{ce}/dt	Time derivative of collector emitter voltage
$\Delta\theta$	Current angle interval
δt	Displacement time
i_c	Semiconductor current
I_{RMS}	Fundamental current
j	Counting variable for number of switching transitions
k	Counting variable incrementing on samples during switching transition
m	Counting variable for random walks
n_1	Lowest number of detectable samples during a switching voltage transition
n_2	Highest number of detectable samples during a switching voltage transition
n_{avg}	Average number of detectable samples during a switching voltage transition
N_{rw}	Number of synthetically generated random walks
N_s	Number of samples
N_{sw}	Number of detected switching transitions
n_{tr}	Number of samples detected during a switching transition
P_1	Probability of sampling n_1 samples during a switching voltage transition
P_2	Probability of sampling n_2 samples during a switching voltage transition
P_{n2}	Probability of sampling $n_1 + 1$ samples during a switching voltage transition (equals P_2)
SEM	Standard Error of the Mean
SEM_{max}	Maximum Standard Error of the Mean
S	Sample
σ	Standard deviation
σ_1	Standard deviation of $\hat{t}_{tr}$
t_0	Time instant
T_j	Semiconductor temperature
T_l	Liquid temperature
$t_{op,max}$	Operational time to reach a desired SEM_{max}
T_s	Sampling time
t_{tr}	Switching transition time
$\hat{t}_{tr}$	Statistially estimated switching transition time
τ	Remaining time
$\hat{t}_{tr,60-120}$	Statistically estimated averaged switching transition time for 60-120 degree interval in current
$\hat{t}_{tr,avg}$	Statistically estimated averaged switching transition time for an arbitrary angle interval in current
v_{max}	Upper detection limit
v_{min}	Lower detection limit
v_{RC}	Rogowski coil voltage
vce	Collector emitter voltage
vce_{on}	On-state collector emitter voltage
vce_{raw}	Collector emitter voltage before signal conditioning
VDC	DC-link voltage

I. INTRODUCTION

IN wind power, a major cost driver for the Operational and Maintenance costs (O&M) is unscheduled maintenance due to unforeseen breakdown of wind turbine components [1].

The complicated logistics related to unscheduled wind turbine maintenance for offshore wind farms is critical. Increasingly remote locations with high wave height and narrow weather windows, coordination of personnel, helicopters and vessels, are challenging factors for the offshore O&M cost structure. The power electronics converter ("converter") is a main source of down time for modern wind turbines [2]–[5],

and the Insulated Gate Bipolar Transistor (IGBT) based power modules ("power modules") of such converters are a major source of converter failures [6]–[8]. Methods of condition monitoring of converters is relevant for bringing O&M cost down [9].

Prediction of emerging power module failures can be achieved by monitoring drifting of operational parameters of power modules and associated gate drives. Several Temperature Sensitive Electrical Parameter (TSEP) detection methods have been proposed during the last decade, as shown in Table I.

The IGBT collector-emitter voltage (vce) switching transition time (t_{tr}) is a TSEP (equivalent to dv_{ce}/dt) and is a candidate for condition monitoring of IGBTs. Contrary to using high precision timing circuitry or very high sample rates, a method is proposed in this paper, which takes a statistical approach to arrive at an estimated switching transition time ($\hat{t}_{tr}$). The proposed method make use of typical voltage measurement circuitry and low sample rates (compared to the signal's rise times), and allows the time between samples (T_s) to be longer than t_{tr}. The accuracy of $\hat{t}_{tr}$ is increased by the number of switching transitions detected (N_{sw}).

The proposed method on statistical estimation of $\hat{t}_{tr}$ is tested on field data, acquired by means of a Converter Monitoring Unit (CMU) which was mounted in the converter of a multi Mega Watt (MW) test wind turbine. The converter of the test wind turbine is a Pulse Width Modulated (PWM), three-phased, two-level converter type. The CMU is a self-sufficient stand alone system which do not require re-design of existing converter designs. It is expected that such self-sufficient CMU may be relevant for retrofitting of existing converters, and may be offered as an option for new converters. Throughout the rest of the paper a description of the monitoring system, description of data handling, and the fundamentals and validity of the statistical method are laid out.

The development and installation of the CMU in the field is part of a cooperation project between a wind turbine converter manufacturer and wind turbine solutions provider (KK Wind Solutions), a leading utility company (Ørsted), and a university (Aalborg University). The aim of the project is to gain required field experience of the CMU for potentially bringing the CMU into large scale implementation in the market for wind turbine converters.

The main contribution of this paper is a method of acquiring the TSEP $\hat{t}_{tr}$ with sample rates orders of magnitude lower than the statistical precision made possible by the method, yet with low hardware (HW) and software (SW) requirements. Simple binning and counting of switching events dramatically reduce the requirement for data storage, processing power, and communication bandwidth, compared to other methods. It is expected that the simplicity of the presented method is an enabler for cost effective converter monitoring solutions, which is a requirement for large scale implementation in the field.

The layout of the paper is as follows: Monitoring of TSEPs are described in Section II. Acquisition of field data are presented, and a description of the CMU is made in Section III. The proposed statistical method is laid out in Section IV,

TABLE I
TEMPERATURE SENSITIVE ELECTRICAL PARAMETERS (TSEP)

No	Method	IGBT	Diode	Reference
1	vce_{on}	x	x	[7], [10]–[18]
2	Turn-off dv_{ce}/dt	x		[19]–[23]
3	Turn-off delay time	x		[24], [25]
4	Turn-on delay time	x		[19]
5	Turn-on di_c/dt	x		[19], [26]
6	Turn-off di_c/dt	x		[25]
7	Reverse recovery charge		x	[27], [28]
8	Internal gate resistor	x		[29], [30]
9	Gate threshold voltage	x		[31]
10	Change of gate voltage and vce_{on}	x		[32]

and tested on field data in Section V. A discussion on the statistical method and it's relevance for condition monitoring in the field, and conclusions on the proposed method are made in Section VI and Section VII, respectively.

II. MONITORING OF TEMPERATURE SENSITIVE ELECTRICAL PARAMETERS

Several TSEP detection methods for IGBTs and diodes have been proposed previously. An overview of such methods are shown in Table I.

The methods of Table I can be explained as:

1) The vce_{on} method refers to sampling of the on-state voltage during conduction of current through the semi-conductor. This method can be used for both the IGBT and parallel diode.
2) Turn-off dv_{ce}/dt method refers to detection of rate of change of the collector-emitter voltage during turn-off of an IGBT. Relevant for the IGBT.
3) Turn-off delay time refers to detection of the time between change of gate signal and actual turn-off of an IGBT. Relevant for the IGBT.
4) Turn-on delay time refers to detection of the time between change of gate signal and actual turn-on of and IGBT. Relevant for the IGBT.
5) Turn-on di_c/dt refers to detection of rate of change of IGBT current during turn-on of an IGBT. Relevant for the IGBT.
6) Turn-off di_c/dt refers to detection of rate of change of IGBT current during turn-off of an IGBT. Relevant for the IGBT.
7) Reverse recovery charge refers to detection of the charge stored in a diode when the complementary IGBT is turned on. Relevant for the diode.
8) Internal gate resistor refers to detection of changes in IGBT on-chip gate resistance due to changes in temperature of the IGBT chip. Relevant for the IGBT.
9) Gate threshold voltage refers to temperature related changes in gate threshold voltage of the IGBT. Relevant

for the IGBT.

10) Change of gate voltage and vce_{on} refers to a method where the gate voltage is changed, and the change of vce_{on} is monitored. Relevant for the IGBT.
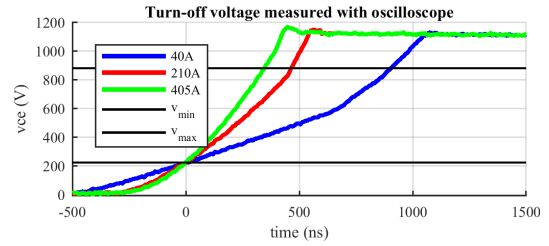

Fig. 1. Collector emitter turn-off voltage measured with oscilloscope in a laboratory. v_{min} and v_{max} defines the lower and upper voltage for switching transition time, and is defined as 20% and 80% of DC-link voltage respectively. Sampling time is 8 ns.

Methods 3 to 10 of Table I require special gate drives or connection to auxilliary terminals of the power modules, and are not relevant for a self-sufficient monitoring system connected to the power terminals of the power modules. The vce_{on} method (method 1 of Table I) was demonstrated in a wind turbine field application for monitoring of both IGBTs and the anti-parallel diodes [10], [11]. vce_{on} is the collector emitter voltage across an IGBT in it's on-state. It was shown that vce_{on} can be monitored by connecting a relatively simple, yet robust measurement circuitry to the collector and emitter terminals of the power modules without the need for special gate drives.

By use of the same connection points as described in [10], [11] (power terminals of the power module), and by allowing the full collector emitter voltage (vce) to be sampled, monitoring of t_{tr} of an IGBT may be enabled (method 2 of Table I). Being able of monitoring two types of TSEPs in essentially the same circuitry expands the monitoring potential of a CMU. The vce sampling equipment and circuitry is further described in Section III-B.

Typically, power modules include heat sink or base plate temperature sensors, but such sensors are only weakly connected to actual semiconductor temperature. This is especially the case for degraded power modules and gate drives. Degradation may occur due to several physical phenomena, but any parameter affecting the thermal properties of the power module, switching behavior of the semiconductors, and potentially also the conduction properties of the power modules may be detected through a TSEP, such as t_{tr}.

Thermal properties of a power module may be degraded due to pump out of thermal interface material [33] or chip solder degradation [34], [35]. Reference [7] found that 7% of an analyzed batch of power stacks failed due to degraded Multi layer Ceramic Capacitors (MLCC) in the gate drive supply circuitry. Failure to MLCCs may lead to open circuit of capacitors or high leakage current [36], which in turn may lead to lowered gate voltage or weak switching performance of the semiconductor. Such changes of the gate drive circuitry will be reflected at the semiconductor as increase of temperature and slowdown of switching voltage transition [37], which can be detected. Several other gate drive related failure modes may also affect t_{tr}, such as too low negative gate supply, which may lead to parasitic turn-on of the complementary IGBT [37], [38], and thus increase of semiconductor temperature.

It has also been proposed that degradation of bond wires may be detected by t_{tr} [39] due to local increase of chip temperature. Local increase of chip temperature due to bond wire fatigue was confirmed in [40], but t_{tr} sensitivity to detecting such failure modes is yet to be investigated, and it is expected that the vce_{on} method is better suited for detecting bond wire fatigue [18], [39]–[44].

A. Detection of Voltage Switching Transition Time

In Fig. 1, the turn-off voltage transition of an IGBT at different current levels are shown. The data were acquired by means of an oscilloscope in a controlled laboratory environment. The IGBT of the laboratory system is equivalent to the IGBTs of the test wind turbine. It is seen in Fig. 1 that the transition time is highly dependent on the current level, with a reduction in switching transition time for increase of current level. For a given current level the transition time tend to increase with increased IGBT temperature [19], [20], [22], [23].

Typically, detecting the rise time of a single turn-off switching transition will require dedicated precision timing circuitry or ADCs with sample rates in hundreds of Mega Samples Per Second (MSPS) to acquire accuracy below 10 nano seconds (ns). Sample rates above 100 MSPS for monitoring of IGBTs was proposed in [45], but the complexity and cost of such circuitry is challenging for a CMU for large scale implementation in the field.

Several Equivalent Time Sampling (ETS) methods are in use in laboratory equipment such as oscilloscopes to increase effective sample rate. Manufacturers use different implementation schemes, which may be referred to as Random Equivalent Time Sampling, Random Interleaved Sampling, Sequential Equivalent Time Sampling, or simply the generic term ETS [46]–[55].

ETS methods require an explicit trigger synchronized to the input signal, and precision timing circuitry to keep track of the time difference between trigger events and sampling events. In addition, ETS require that the waveform to be sampled is repeated sequentially. Fulfilling the above requirements, ETS methods can reconstruct wave forms by means of a sampling frequency lower than the frequencies embedded in the recovered signal.

Compressed Sensing methods (CS) which goes against the normal practice in data acquisition (e.g. the so-called Nyquist rate which requires a sampling rate at least twice the maximum frequency in the signal), is becoming increasingly popular [56]. In applications such as surface metrology [57], photography [58], Magnetic Resonance Imaging (MRI) [59], astronomy [60], and even condition monitoring of IGBTs [23], CS have proven efficient in reconstructing drastically undersampled data. Typical CS methods involve transformation of the sampled data from a basis in the time domain to a basis in the frequency domain, such as Fourier basis or one of several

wavelet bases [23], [56].

With only a few ns of error, [23] demonstrated successful reconstruction of IGBT vce switching wave forms by compressing raw signals of 1 Giga Samples per Second (GSPS) to 25 MSPS (compression ratio of 40). Compared to 1 GSPS, 25 MSPS is obviously a major reduction in the sampling requirement for such measurement system, but it is expected that even a 25 MSPS system may be of too high sample rate for a commercial converter monitoring system, due to the cost of the hardware and the amount of data which must be processed.

With sampling intervals (T_s) which may be close to, or even longer than t_{tr}, the frequency information embedded in the switching transition is not accessible, making CS inappropriate.

A statistical approach for t_{tr} detection is proposed in this paper, which requires multiple switching transitions of comparable t_{tr} as input. As will be further explained in the following sections, the proposed method requires that switching transitions occur at random time instants relative to the sampling intervals, which equivalates the ETS methods' random or sequential distribution of sampling intervals relative to trigger instants.

Contrary to the ETS methods, the proposed method does not require a synchronized trigger and precision timing circuitry to track the time difference between trigger instants and sampling instants. Further, the proposed method does not require that equal switching transitions are repeated sequentially, as required by the ETS methods. In the proposed method the requirement for multiple switching transitions can easily be handled by simple updating of counters, as will be further explained in Section III-C.

Finally, the proposed method does not require that raw sample values are stored, since the calculation scheme only requires updating of counter values. Hence, the HW and SW requirements for the proposed method are drastically reduced compared to previously presented methods such as ETS and CS. Contrary to ETS and CS methods, the proposed method cannot reconstruct the waveform of the input signal, only the switching transition time is calculated, which is sufficient for using t_{tr} as a TSEP for monitoring of semiconductors.

Assuming sampling of vce during multiple switching transitions with equal t_{tr}, the estimated $\hat{t}_{tr}$ can be calculated by simple counting of number of samples detected during the switching transitions ($n_{tr}(j)$) divided by the total number of switching transitions (N_{sw}) as of (1), where j is a counting variable for number of switching transitions.

$$\hat{t}_{tr} = \frac{\sum_{j=1}^{N_{sw}} n_{tr}(j)}{N_{sw}} \cdot T_s \qquad (1)$$

In Section IV it will be shown that $\hat{t}_{tr}$ converges towards a fixed value as the number of detected switching transitions (N_{sw}) are increased , and that the deviation (error) in relation to the final value decrease towards higher numbers of N_{sw}.

III. DATA ACQUISITION IN THE FIELD

Modern MW sized wind turbines for onshore and offshore operation are equipped with Doubly-Fed Induction Generators
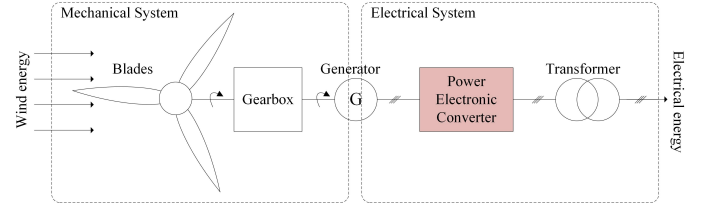

Fig. 2.   Basic wind turbine diagram utilizing full scale power conversion.
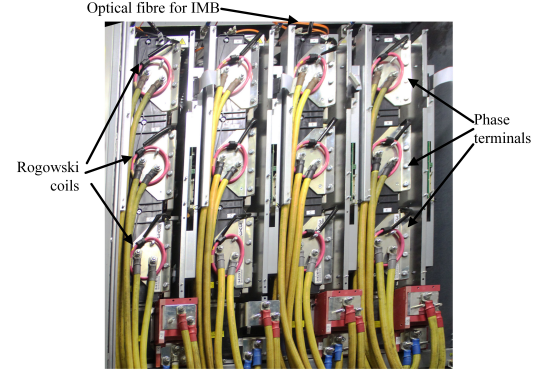

Fig. 3.   Machine Side Converter of test wind turbine.

(DFIG), Permanent Magnet Synchronous Generators (PMSG), Squirrel Cage Induction Generators (SCIG), or Electrically Excited Synchronous Generators (EESG) [61]. To control the torque of the generator and to convert the variable frequency/variable voltage of the generator, a power electronics converter is required. A basic wind turbine diagram for full scale converters (relevant for PMSG and SCIG) is shown in Fig. 2.

A. Wind Turbine Converter

The converter of the test wind turbine is a two-level full scale back-to-back converter, connected to a SCIG. The converter consist of a Machine Side Converter (MSC) and a Line Side Converter (LSC). Both the MSC and LSC are three-phased converters with four power modules in parallel per phase, grouped in four parallel connected "power stacks" per converter. A picture of the MSC is shown in Fig. 3. Parallel power modules are separated by sharing reactors with inductance values of several micro Henry. Hence, differences in switching transition times between parallel power modules are of little impact for the switching transition itself, but may alter current sharing between the parallel power modules. Generic information on wind turbine converters are found in [62].

B. Retrofitted Converter Monitoring Unit (CMU)

At each power module of the converter is mounted an IGBT Measure Board (IMB) to sample the power module signals, as shown in the single-line diagram of the back to back converter of Fig. 4 and power stack photo of Fig. 5.

For each IGBT/diode pair of the converter, the physical raw collector-emitter voltage (vce_{raw}) is split into a vce_{on} signal
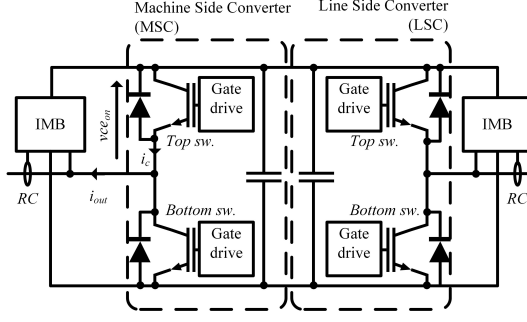
Fig. 4. Single-line diagram of back to back converter. At each power module an IGBT Measure Board (IMB) is mounted, referring to the middle point of the half bridge.
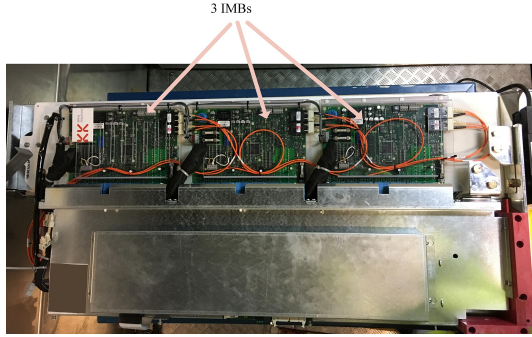

Fig. 6. Basic IGBT Measure Board (IMB) circuitry.

Fig. 5. Three IGBT Measure Boards (IMBs) mounted on a three phased power stack.

and a vce signal, which are both sampled by means of embedded Analog to Digital Converters (ADC) and multiplexers (MUX) in a micro controller (μC), as shown in Fig. 6.

The vce_{on} circuitry enables high ADC resolution in the conduction mode, but saturates when voltage goes beyond $\pm$ 5V, as described in [10]. The vce circuitry allows for sampling of the vce voltage in it's full voltage range, yet with lower resolution in absolute voltage. Rogowski coils (RC) are used for sampling of semiconductor current (i_c). RC outputs a voltage (v_{RC}) which is proportional to the time derivative of the current (di_c/dt), and an integration of the signal must be performed to arrive at i_c. The raw rogowski coil voltage is numerically integrated, as described in [10].

Due to the nature of the test project, all processing of data from the CMU is performed off-line. Such off-line data processing is demanding for the communication bandwidth and data storage requirements. As part of a potential commercialization of the CMU, both the electronics HW and mechanics will be optimized. Implementation of data processing in the CMU is a major part of such optimization. In the following sections the implications of on-line data processing are discussed, but not performed. Based on experience gained from the test project, strategies for drastically reducing the mounting complexity have been addressed, but is out of scope for this paper.

The μC of the IMB have two main processor cores and two co-processor cores. In one of the co-processor cores, pre-processing of the vce_{on} data is performed. It is expected that in an optimized implementation, the other co-processor core
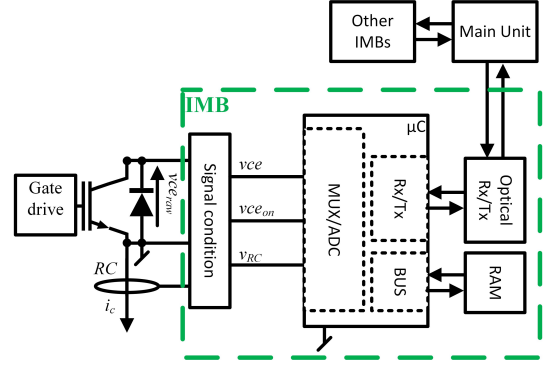
can perform processing of the vce data, such as detection of switching transitions and counting samples being in the transitions, according to (1). Such pre-processing will drastically reduce the data memory requirements and communication bandwidth requirements, and thereby fully exploit the simplicity of the proposed method. Actual implementation in the μC was not a scope for the test project. Through optical fibers, the IMBs communicate with a main unit which stores sampled data and transmits the data to a cloud server for post processing of the data.

All analog signals (vce_{on}, vce , and v_{RC}) for all IMBs are sampled with $T_s = 1.88\mu s$ continuously and saved in ring buffers. Every 10 minutes the data in the ring buffers are transmitted to a cloud server. One set of such data is referred to as a "log" and contains data of approximately 0.4 seconds duration. The converter is liquid cooled. The liquid coolant temperature (T_l) is monitored in the wind turbine Supervisory Control and Data Acquisition system (SCADA), and paired with CMU data in post processing.

C. Grouping of Data

The methods of estimating $\hat{t}_{tr}$ according to (1) rely on sampling vce during multiple pulses of comparable t_{tr}. Physical t_{tr} depends on instantaneous semiconductor current and semiconductor chip temperature (T_j), which will vary continuously in a wind turbine converter. The variation of the instantaneous current is most prominent during the current trajectory of the sinusoidal current, which will lead to different instantaneous current levels between two subsequent switching transitions, as can be seen in Fig. 7. The chip temperature will vary as a function of fundamental current (I_{RMS}) and T_l (or air-temperature for air-cooled converters). I_{RMS} vary as a function of wind dynamics, wind turbine and converter control strategy, generator properties, and grid voltage. T_l will be determined by the cooling control strategy, which is influenced by the ambient temperature and I_{RMS}.

Due to the constantly varying parameters i_c, I_{RMS}, and T_l during operation, sampled data must be grouped according to the same parameters, so that estimation of $\hat{t}_{tr}(i_c, I_{RMS}, T_l)$ can be performed in accordance with (1). Instantaneous current and fundamental current are correlated, which means that the sample space $\hat{t}_{tr}(i_c, I_{RMS}, T_l)$ can be reduced to an averaged sample space $\hat{t}_{tr,avg}(I_{RMS}, T_l)$. $\hat{t}_{tr,avg}$ represents
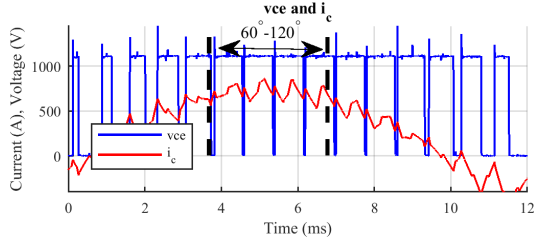
Fig. 7. Phase current (i_c) and collector-emitter voltage (vce) for one power module of converter during approximately half fundamental period.

Fig. 8. Sampling of vce during a switching transition. The solid trajectory shows a switching transition starting at time t_0. The dotted trajectories show switching transitions with starting times offset to t_0. Vertical dotted lines denote sampling intervals.

the averaged estimated $\hat{t}_{tr}$ during a defined portion of the fundamental current wave, e.g. between 60 and 120 degrees in the current angle (interval marked by dotted lines in Fig. 7). The 60 to 120 degree span may be chosen as a practical compromise between having a long summation interval and small variation of current amplitude. In the following sections $\hat{t}_{tr,60-120}(I_{RMS}, T_l)$ from the test wind turbine are used, which are the averaged $\hat{t}_{tr}$ in the 60-120 degree interval of the current. The field data are grouped in 50A intervals on I_{RMS} and 5°C intervals on T_l. By implementing the methods of this paper in the CMU itself, saving of raw data is not required. For each I_{RMS}, T_l combination, two counting values are required, representing N_{sw} and $\sum_{j=1}^{N_{sw}} n_{tr}(j)$ as of (1). With 50A intervals on I_{RMS} in the range 50A to 1000A, and 5°C intervals on T_l in the range 25°C to 55°C, the required number of counting values are $2 \cdot 7 \cdot 20 = 320$.

D. Test Campaign

During a 3 month test campaign, approximately 11000 logs from the CMU were stored, representing raw data from approximately 4400 seconds of data acquisition (referred to as "operational time" in the following). I_{RMS} and T_l varied as function of control parameters and wind input to the wind turbine. In the following sections, "field data" are referring to data from one IGBT of a power module of the MSC sampled during the test campaign.

IV. STATISTICAL METHOD

The CMU samples vce continuously with a sample interval T_s, without any synchronization to the PWM voltages of the converter. T_s is chosen arbitrarily in relation to the switching frequency of the converter. The converter PWM voltages vary constantly due to varying voltage angle, wind perturbations on the generator, voltage variations in the grid and other disturbances related to the control of the converter. In addition, the PWM pattern is not synchronized to the fundamental of the modulated voltage of the converter.

The statistical method laid out in the following thus presumes that the sampling of the vce in the CMU are at fixed intervals, but the switching transitions occur at random time instants relative to the sampling intervals. By analyzing already sampled data in a log, the occurrence of switching transitions can be detected, even in cases when no samples are performed in the switching transition itself. A turn-off switching transition is detected when sampled vce go from

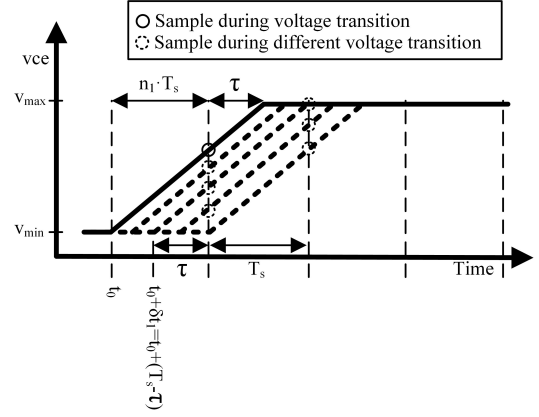low values to high values (turn-on switching transitions occur at vce samples going from high values to low values). When such a switching transition is detected, the number of samples performed during the switching transition is counted, and the switching transition event is also counted, according to (1). Hence, separate HW triggering of switching events are not required.

The method described only use the samples which are registered as being in the transition. Samples which are not in the transition are discarded.

A turn-off switching event is visualized in Fig. 8, where the vce voltage rises between v_{min} and v_{max}, defined as zero volts and VDC respectively. In the physical converter, switching transitions lead to oscillations in parasitic elements in the DC-link, which may lead to false detection of switching transitions. Therefore v_{min}, v_{max} should be defined at levels which are not affected by the parasitic oscillations. Choice of v_{min}, v_{max} are compromises between robustness margins for false detection and estimation accuracy. In the application, v_{min}, v_{max} values of 20% and 80% of VDC were used.

The vertical dashed lines denotes time instants where the CMU samples vce, and the circles denote samples which are used.

As described above, there is no synchronization between switching events and sampling of vce, but assume that a switching transition is started at time instant t_0, where t_0 occur immediately after a vce sampling has been performed. Assume for a given t_{tr} and T_s that the relation of (2) holds, where n_1 is an integer and τ is a remainder.

$$t_{tr} = n_1 \cdot T_s + \tau, \ \tau < T_s \qquad (2)$$

As an example, consider the case of $n_1 = 1$ so that $t_{tr} = T_s + \tau$. The special case of a switching transition starting at time t_0, is shown in the example of Fig. 8 (solid line), where one positive sample is obtained (a sample is positive if it is performed during t_{tr}). Since the voltage transition can occur at random time instants relative to the sampling intervals, the voltage transition can start at time t_0 added any random

displacement time δt, as $t_0 + \delta t$. In Fig. 8, different switching trajectories, starting at different $t_0 + \delta t$ instants are visualized as dotted lines . As may be observed, the sample count will remain at $n_1 = 1$ as long as $\delta t < (T_s - \tau)$. For $(T_s - \tau) < \delta t < T_s$ one additional sample compared to n_1 will be performed during the switching transition, so total sample count is $n_2 = n_1 + 1$ for such transitions. The borderline between n_1 and n_2 samples is shown at $t_0 + \delta t_1 = t_0 + (T_s - \tau)$ of Fig. 8. Due to the periodicity of the sampling instants, cases of $T_s < \delta t$ can be reduced to the cases already discussed. Thus, n_1 samples will be performed for $\delta t < (T_s - \tau)$ and n_2 samples will be performed for $(T_s - \tau) < \delta t < T_s$.

From (2), n_1 can be calculated as (3), and n_2 can be calculated as (4).

$$n_1 = \frac{t_{tr}}{T_s} - \frac{\tau}{T_s} = \lfloor \frac{t_{tr}}{T_s} \rfloor = floor \left(\frac{t_{tr}}{T_s} \right) \quad (3)$$

$$n_2 = n_1 + 1 = \lceil \frac{t_{tr}}{T_s} \rceil = ceil \left(\frac{t_{tr}}{T_s} \right) \quad (4)$$

As a consequence of the fixed periodic sampling occurrence of T_s, the probability of a given sample being positive (sampled during t_{tr}) depends on the previous and/or subsequent samples since t_{tr} represent a continuous interval. For a given t_{tr} and T_s either n_1 samples or n_2 samples will be performed.

Let k be a counting variable which is reset to 0 on samples before t_{tr}, and is incremented on samples performed after start of t_{tr}. The probability of a sample $S(k)$ being positive can be written as:

$S(k) = 1$ with probability 1 if $k \leq n_1$
$S(k) = 1$ with probability P_{n2} if $k = n_1 + 1 = n_2$
$S(k) = 0$ with probability $(1 - P_{n2})$ if $k = n_1 + 1 = n_2$
$S(k) = 0$ with probability 1 if $k > n_2$

The probability (P_{n2}) of sampling the $n_1 + 1 = n_2$ sample during a voltage transition is the ratio between τ and T_s, as of (5).

$$P_{n2} = \frac{\tau}{T_s} \quad (5)$$

Now that the probabilities for $S(k)$ are defined, the probability of sampling n_2 successive positive samples ($P2$) can be defined as (6). The probability of only sampling n_1 successive positive samples ($P1$) can thus be defined as (7).

$$P2 = \left(\prod_{k=0}^{n_1} 1 \right) \cdot P_{n2} = P_{n2} = \frac{\tau}{T_s} = \frac{t_{tr}}{T_s} - n_1 \quad (6)$$

$$P1 = \left(\prod_{k=0}^{n_1} 1 \right) \cdot (1 - P_{n2}) = 1 - \left(\frac{t_{tr}}{T_s} - n_1 \right) = n_2 - \frac{t_{tr}}{T_s} \quad (7)$$

By defining the average number of samples (n_{avg}) during a switching transition with a given t_{tr} and T_s as (8), equations (6) and (7) can be written as (9) and (10).

$$n_{avg} = \frac{t_{tr}}{T_s} \quad (8)$$
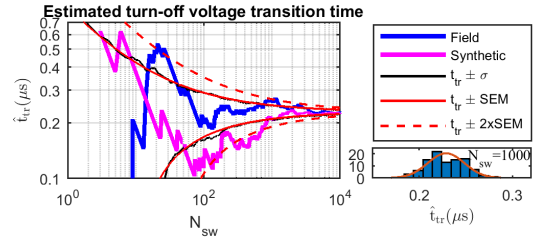
$$P_1 = |n_2 - n_{avg}| \quad (9)$$

Fig. 9. Estimation of switching transition time for field data, compared to synthetic data.

$$P_2 = |n_1 - n_{avg}| \quad (10)$$

It is expected that $\hat{t}_{tr}$ approaches the physical t_{tr} as N_{SW} approaches large values. Now that the fundamentals regarding number of samples (n_1, n_2) during t_{tr} and their respective probabilities (P_1, P_2) are defined, the statistical error on (1) as a function of N_{sw} can be laid out.

A. Standard Error of the Mean (SEM)

A series of switching transitions may be considered a "random walk", where the δt of a switching event (j) is random, but the calculation of $\hat{t}_{tr}(N_{sw})$ according to (1) is dependent on the switching event and all previous switching events of the random walk. One such random walk is shown in Fig. 9 (magenta), where the underlying data are generated synthetically (simulated) by a random generator on a computer. The simulated switching transitions are calculated by randomly generating $n_{tr}(j)$ according to the probabilities (9) and (10), which allows calculation of the simulated $\hat{t}_{tr}(N_{sw})$.

By performing a high number (N_{rw}) of synthetically random walks one can investigate how $\hat{t}_{tr}(N_{sw})$ spreads as a function of N_{sw}. A set of simulations were performed with $N_{rw} = 100$, $N_{sw} = [1, 1e4]$. The "physical" t_{tr} used for the synthetically random walks, is the final value of the $\hat{t}_{tr}$ estimations at 800 A from field data, shown in Fig. 9. For each value of N_{sw}, the standard deviation of the random walks ($\sigma(N_{sw})$) of the simulated $\hat{t}_{tr}(N_{sw}, m)$ were calculated (m is a counting variable for random walks).

The obtained population of results of such independent random walks calculated according to (1) should tend towards a normal distribution in line with the Central Limit Theorem. It is thus expected that the distribution of $\hat{t}_{tr}$ will tend towards normal distribution. Indeed, in the inset of the lower right corner of Fig. 9, the distribution of $\hat{t}_{tr}(N_{sw} = 1000)$ for the 100 synthetic random walks is shown, which clearly indicates a normal distribution of the $\hat{t}_{tr}$ estimations. The standard deviation as function of N_{sw} ($\sigma(N_{sw})$) is plotted in Fig. 9.

The error on $\hat{t}_{tr}$ can be calculated analytically as the standard error of the mean (SEM). According to [63], standard error is defined as "the standard deviation of the sampling distribution of a statistic", and is calculated as (11). σ_1 is the standard deviation of $\hat{t}_{tr}$ for one switching transition.

$$SEM(N_{sw}) = \frac{\sigma_1}{\sqrt{N_{sw}}} \quad (11)$$

With normal distributed data, $\pm\sigma$ contains approximately 68% of the random walks, and $\pm 2\cdot\sigma$ contains approximately 95% of the random walks. Equally, approximately 68% of the $\hat{t}_{tr}$ estimates are expected to be within the $\pm SEM$ envelope of Fig. 9 (red), and approximately 95% of the $\hat{t}_{tr}$ estimates are expected to be within the $\pm 2\cdot SEM$ envelope (dashed red) of Fig. 9. It can be observed that the analytical $\pm SEM$ envelope closely resembles $\pm\sigma$ on the synthetically generated random walks shown in Fig. 9. It can also be observed that the trajectory of the synthetically generated random walk displayed in Fig. 9 (magenta) resemble the same quantitative and qualitative properties as the random walk of switching transitions from the field data (blue). Together with the fact that the $\hat{t}_{tr}$ estimates tend to follow a normal distribution, it can be concluded that the analytical SEM is a good approximate of the error on the estimated $\hat{t}_{tr}$ as a function of N_{sw}. In the following the analytical parameters required for calculating SEM are laid out.

Based on the definition of standard deviation, the standard deviation of $\hat{t}_{tr}(N_{sw}=1)$ for N_{rw} random walks is thus defined as (12). N_{rw} is the number of random walks, m is a counting variable for random walks.

$$\sigma_1 = \sqrt{\frac{1}{N_{rw}}\cdot\sum_{m=1}^{N_{rw}}\left((n_{tr}(m)-n_{avg})\cdot T_s\right)^2} \qquad (12)$$

Instead of calculating σ_1 based on empirical N_{rw} random walks, σ_1 can be calculated based on the probabilities of arriving at n_1 samples ($P1$), or n_2 samples ($P2$) during a switching transition, since these are the only two outcomes at given t_{tr} and T_s. Equation (12) can thus be rearranged into (13).

$$\sigma_1 = \sqrt{P_1\cdot\left((n_1-n_{avg})\cdot T_s\right)^2 + P_2\cdot\left((n_2-n_{avg})\cdot T_s\right)^2}$$
$$= \sqrt{P_1\cdot(P_2\cdot T_s)^2 + P_2\cdot(P_1\cdot T_s)^2}$$
$$(13)$$

For a given T_s, $SEM(N_{sw})$ will be dependent on the physical t_{tr}, but the maximum possible $SEM(N_{sw})$ for a given T_s can be calculated and used for worst-case calculations for varying t_{tr}, or if expected t_{tr} is not known. The maximum possible $SEM(N_{sw})$ for the given T_s is referred to as $SEM_{max}(N_{sw})$. The highest value of σ_1 (referred to as $\sigma_{1,max}$) for a given T_s will be met when $P_1 = P_2 = 1/2$. Rearranging (13) into (14) allows for calculation of $SEM_{max}(N_{sw})$ as of (15).

$$\sigma_{1,max} = \sqrt{\left(\tfrac{T_s}{2}\right)^2/2 + \left(\tfrac{T_s}{2}\right)^2/2}$$
$$= \frac{T_s}{2} \qquad (14)$$

$$SEM_{max}(N_{sw}) = \frac{\sigma_{1,max}}{\sqrt{N_{sw}}}$$
$$= \frac{T_s}{2\cdot\sqrt{N_{sw}}} \qquad (15)$$

Rearranging (15), one can calculate the number of switching transitions required for a given SEM_{max}, as of (16).

$$N_{sw}(SEM_{max}) = \left(\frac{T_s}{2\cdot SEM_{max}}\right)^2 \qquad (16)$$

It is seen from (15) that $SEM_{max}(N_{sw})$ depend linearly on T_s, but on the square root of N_{sw}, which favors decrease of T_s (increase of sampling frequency) compared to increase of number of switching transitions.

B. Operational Time

In Section III-C it was described that the field data must be grouped according to i_c, I_{RMS}, T_l, and it was proposed to correlate i_c and I_{RMS} by averaging of $\hat{t}_{tr}$ in a defined current angle interval ($\Delta\theta$) (e.g. between 60 and 120 degrees). Such averaged $\hat{t}_{tr}$ is referred to generically as $\hat{t}_{tr,avg}$ and specifically as $\hat{t}_{tr,60-120}(I_{RMS}, T_l)$ for the 60 to 120 degree interval. By taking $\Delta\theta$ and the switching frequency of the converter (f_{sw}) into account, (16) can be expanded to (17), where $t_{op,max}(I_{RMS}, T_l)$ is the operational time required to reach a desired SEM_{max} for a given load point. Equation (17) is defined for continuous PWM at a fixed switching frequency.

$$t_{op,max}(I_{RMS}, T_l) = N_{sw}(SEM_{max})\cdot\frac{2\cdot\pi}{f_{sw}\cdot\Delta\theta}$$
$$= \left(\frac{T_s}{2\cdot SEM_{max}}\right)^2\cdot\frac{2\cdot\pi}{f_{sw}\cdot\Delta\theta} \qquad (17)$$

For the MSC of the test turbine, $t_{op,max}(I_{RMS}, T_l)\approx 3600s$ (1 hour) when operating at $f_{sw} = 1250$ Hz, $T_s = 1.88\ \mu s$, $SEM_{max} < 1.1$ ns, and $\Delta\theta = \pi/3$ (averaging between 60 and 120 degrees in current angle).

With the data acquisition scheme described in Section III, actual time is much longer than operational time. In case of continuous sampling and calculation in a CMU, $t_{op,max}(I_{RMS}, T_l)$ equals the actual time. Such optimization of the data acquisition scheme is further discussed in Section VI.

V. STATISTICAL METHOD TESTED ON FIELD DATA

Condition monitoring of power modules enable detection of anomalies, and thereby potentially detection of emerging power module and gate drive failures. Reference data (calibration data) for each semiconductor are required in order to calculate change of semiconductor temperature for a given load point. References [10], [11] have shown that such individual reference data can be generated in a field application without special calibration equipment or calibration routines.

By monitoring changes of T_j relative to reference data, degradation of the power modules or gate drives may be detected [10], [11]. The methods of [10], [11] do not require knowledge of T_j, but tracking of relative variation of T_j in the whole operational range can be performed. It is expected that the reference data generation methods of [10], [11] can be adapted for use with the $\hat{t}_{tr}$ estimation method proposed in this paper, but such adaptation is not further evaluated.

In the following sections, the fundamental properties of the proposed statistical method applied to field data are examined.
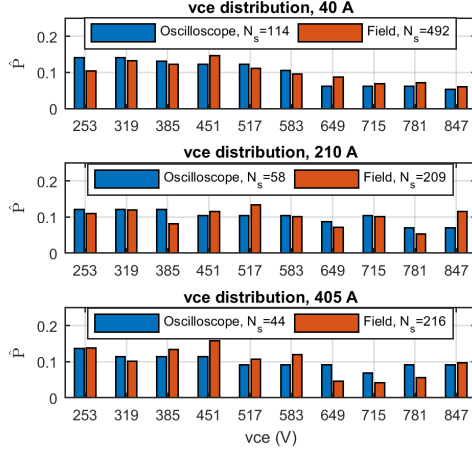
Fig. 10. Compared distribution of vce during switching voltage transition for vce sampled in the field and vce sampled by means of oscilloscope. Samples of vce are grouped in ten equally spaced intervals between v_{min} and v_{max} and samples are counted. The numbers on x-axis denote the middle of the vce intervals.
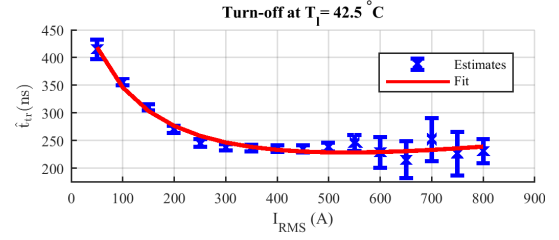

Fig. 11. Turn-off estimation of $\hat{t}_{tr,60-120}$ as function of fundamental current (I_{RMS}) for one IGBT of the MSC of the field test turbine. Error bars equal Standard Error of the Mean (SEM).
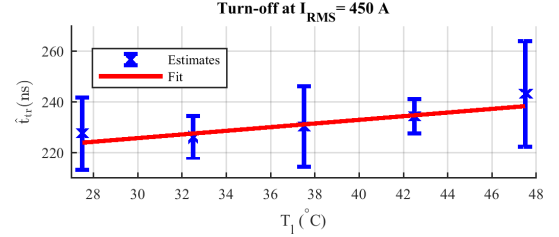

Fig. 12. Turn-off estimation of $\hat{t}_{tr,60-120}$ as function of liquid coolant temperature (T_l) for one IGBT of the MSC of the field test turbine. Error bars equal Standard Error of the Mean (SEM).

A. Testing of Random Distribution in Field Data

To test the assumption of random distribution of δt (discussed in Section IV), histogram plots of sampled vce during switching transitions in field data are compared to histogram plots of oscilloscope data from single switching events in a laboratory test setup. Data from the field and laboratory with comparable i_c, I_{RMS} and T_l are grouped in ten equally spaced vce intervals between v_{min} and v_{max}, and counted. The voltage levels v_{min}, v_{max} are defined as 20% and 80% of VDC (1100V).

Such comparison is shown in Fig. 10. The blue bars of Fig. 10 show the distribution of vce from the oscilloscope data of Fig. 1. The red bars of Fig. 10 show vce distribution of field data which are grouped according to $i_c = i_{c,ref} \pm 5A, I_{RMS} = 300A \pm 25A, T_l = 45°C \pm 2.5°C$. $i_{c,ref}$ equals the instantaneous current levels shown in Fig. 1 (40A, 210A, and 405A).

Comparing the voltage distribution for time-sampled oscilloscope data during single switching transitions (blue bars) to random-time sampled field data during multiple switching transitions (red bars) show comparable voltage distribution for the three current levels in Fig. 10. The number of samples for each group of data are denoted N_s in Fig. 10. It is seen that for the higher current values (210A and 405A) only slightly above 200 samples are stored in the field data, indicating that the data are randomly distributed even for small number of samples. It can thus be concluded that the assumption of randomness on δt is valid.

B. Current and Temperature Dependency on $\hat{t}_{tr}$

Results of $\hat{t}_{tr,60-120}(I_{RMS},T_l)$ calculations for turn-off based on field data, are shown in Fig. 11 and Fig. 12. The error bars in the plots are calculated as $\pm SEM$, as of (11), based on the estimated $\hat{t}_{tr,60-120}(I_{RMS},T_l)$. The turn-off rise time is defined as the time duration between 20% and 80%

of the DC-link voltage (VDC) during switching. VDC is constant at 1100V during the whole test campaign.

In the data underlying Fig. 11 and Fig. 12, T_j is not known. T_j is related to T_l, IGBT losses (correlating with I_{RMS}) and the thermal impedance between semiconductor chips and liquid coolant. As I_{RMS} increases, T_j relative to T_l tend to rise due to increase of conduction and switching losses of the IGBT. The actual T_j at high I_{RMS} of Fig. 11 is thus higher than actual T_j at low I_{RMS}. The temperature sensitivity shown in Fig. 12 is expected to represent the actual t_{tr}/T_j sensitivity, since an elevation of the liquid temperature will lead to approximately equal elevation of junction temperature for a given I_{RMS} (actual T_j will increase slightly more than increase of T_l due to increase of power losses, but can be neglected for practical purposes).

Typical turn-off characteristics of IGBTs show a decrease in t_{tr} as function of increase of i_c, yet increase of t_{tr} as function of increase of T_j [19], [20], [22], [23], which is shown clearly in Fig. 11 and Fig. 12. It should be noted that during the test campaign (summer), the wind conditions favored low power operation, so at the higher current levels the number of detected switching transitions are sparse, leading to relatively high estimation errors on $\hat{t}_{tr,60-120}$ at high current levels of Fig. 11. Hence, the relatively high estimation errors at high current values are results of the seasonal variation in wind conditions and not an indication of higher estimation errors at higher current levels.

By implementing on-line calculation of $\hat{t}_{tr,60-120}$ in the CMU itself, the estimation errors can be reduced drastically due to a higher number of N_{sw} acquired, as will be discussed further in Section VI. The temperature sensitivity on $\hat{t}_{tr,60-120}$ is clearly seen in Fig. 12, where the fitted temperature sensitivity is approximately $0.8 ns/°C$. With an on-line calculation

scheme, the estimation errors of Fig. 12 can also be reduced.

VI. DISCUSSION

The off-line data acquisition and processing scheme described in Section III stores 0.4 seconds of data every 10 minutes, which means that only $^1/_{1500}$ of physical switching transitions are processed. With continuous on-line processing of sampled data, one should arrive at $\hat{t}_{tr}$ estimations in a shorter actual time and/or with a higher precision.

Calculation of $\hat{t}_{tr,60-120}(I_{RMS}, T_l)$ is of relatively low complexity, and can potentially be implemented in the CMU for continuous processing of switching transition samples. Such on-line calculation scheme also reduces the requirement for saving of raw samples, and as a consequence will reduce communication bandwidth requirements. With $T_s= 1.88~\mu s$, as of the test campaign, $\hat{t}_{tr,60-120}(I_{RMS}, T_l)$ calculation requires approximately one hour of operational data for a given load point (see Section IV-B), which will equal actual time if the CMU performs continuous processing of switching transitions. The one hour requirement is for a defined precision of $SEM_{max} < 1.1ns$, which approximates a temperature error of $\pm 1.4°C$ (0.8ns/°C). Reducing the estimation accuracy will impact $t_{op,max}(I_{RMS}, T_l)$ quadratically according to (17). By defining $SEM_{max} < 11ns$ (temperature error of approximately $\pm 14°C$), $t_{op,max}(I_{RMS}, T_l) \approx 36s$.

The ADCs of the CMU can sample up to 3.5 MSPS ($T_s= 286$ ns). According to (17), optimizing the ADC conversion scheme to 3.5 MSPS will result in $t_{op,max}(I_{RMS}, T_l) \approx 83s$ for the high precision of $SEM_{max} < 1.1ns$. By increasing the sample rate to 3.5 MSPS in combination with the lower precision of $SEM_{max} < 11ns$, the operational time for a given load point is reduced to 0.83s, according to (17).

Slow changes of the power module and gate drive parameters due to deterioration of the power module semiconductors, bond-wires, power module thermal interface, or gate drives, may thus be detected with high accuracy in minutes or hours of operational time. Rapid changes of the power module and gate drive parameters due to overload, grid transients etc., may be performed in seconds or sub second detection time, with reduced accuracy.

According to (1), variation on T_s will affect $\hat{t}_{tr}$ according to the ratio on T_s variation, and thus makes the proposed method robust against variations on crystal oscillator frequency. As an example, consider a crystal oscillator tolerance of 0.2% and a physical $t_{tr} = 250$ ns. The tolerance on $\hat{t}_{tr}$ will be $0.2\% \cdot 250\,\text{ns} = 0.5\,\text{ns}$, which corresponds to less than $0.63°C$ (0.8ns/°C). With a linear t_{tr} curve, change in offset voltage in the vce circuitry will be eliminated in the $\hat{t}_{tr}$ estimation. For non-linear t_{tr} curves, change of offset values may result in minor impact on $\hat{t}_{tr}$. Tolerances in the gain of the analog vce sampling circuitry will affect $\hat{t}_{tr}$ in accordance with tolerance on $v_{max} - v_{min}$.

Compared to other methods, the disadvantages of the proposed method include the lack of possibility to reconstruct the shape of the switching voltage waveform, and $\hat{t}_{tr}$ cannot be detected on single switching transitions. The requirement for multiple switching transitions eliminates the possibility to react to immediate temperature changes of the power module semiconductors. As discussed above, detection times can be reduced to only a few seconds, and reconstruction of voltage waveform is not required for condition monitoring. Hence, the disadvantages of the proposed method is of minor relevance for condition monitoring of IGBTs in a wind turbine converter.

VII. CONCLUSION

In this paper a method of estimating IGBT switching voltage transition time based on a statistical approach was presented and tested on field data from a test wind turbine converter. The distribution of the errors on synthetically generated random walks correspond to the analytical calculations of the Standard Error of the Mean (SEM), which can thus be used for calculation of expected error on $\hat{t}_{tr}$. The proposed method is relevant for low-cost monitoring systems for field operated converters, where detection of switching transition times can be performed in minutes to hours with high precision, or detection times in seconds or sub seconds with reduced accuracy.

REFERENCES

[1] A. Scassola, "Offshore wind o&m market dynamics in europe," *MAKE (A Wood Mackenzie Business) Research Note. 21. Dec. 2015.*

[2] F. Spinato, P. J. Tavner, G. J. W. V. Bussel, and E. Koutoulakos, "Reliability of wind turbine subassemblies," *IET Ren. Pow. Gen.*, vol. 3, no. 4, pp. 387–401, 2009.

[3] M. Wilkinson, K. Harman, B. Hendriks, F. Spinato, T. van Delft, G. Garrad, and U. Thomas, "Measuring wind turbine reliability-results of the reliawind project," *EWEA Conference*, 2011.

[4] F. Besnard, "On maintenance optimization for offshore wind farms," Ph.D. dissertation, Phd thesis 2013.

[5] J. Carroll, A. McDonald, and D. McMillan, "Reliability comparison of wind turbines with dfig and pmg drive trains," *IEEE Transactions on Energy Conversion*, vol. 30, no. 2, pp. 663–670, 2015.

[6] K. Fischer, T. Stalin, H. Ramberg, T. Thiringer, J. Wenske, and R. Karlsson, "Investigation of converter failure in wind turbines. [online]:," Elforsk, Tech. Rep. 12:58, 2012. [Online]. Available: https://www.researchgate.net/profile/Jan_Wenske/publication/279511307_Investigation_of_converter_failure_in_wind_turbines/links/5593d1e508aed7453d46d144.pdf

[7] B. Rannestad, A. E. Maarbjerg, K. Frederiksen, S. Munk-Nielsen, and K. Gadgaard, "Converter monitoring unit for retrofit of wind power converters," *IEEE Trans. Pow. El.*, vol. 33, no. 5, pp. 4342–4351, May 2018.

[8] K. Fischer, K. Pelka, A. Bartschat, B. Tegtmeier, D. Coronado, C. Broer, and J. Wenske, "Reliability of power converters in wind turbines: Exploratory analysis of failure and operating data from a worldwide turbine fleet," *IEEE Transactions on Power Electronics*, pp. 1–1, 2018.

[9] S. B. Nielsen, "Make (a wood mackenzie business) service market survey [online]," 19-20 April 2016. [Online]. Available: http://aea-al.org/wp-content/uploads/2016/06/160502_SKF_WFMC_Polling_Results_2016_public_version.pdf

[10] B. Rannestad, P. Nielsen, S. Munk-Nielsen, K. Gadgaard, and S. Jorgensen, "Converter monitoring in a wind turbine application," *Microelectronics Reliability*, vol. 88-90, pp. 1008 – 1013, 2018.

[11] B. Rannestad, K. Fischer, P. Nielsen, K. Gadgaard, and S. Munk-Nielsen, "Virtual temperature detection of semiconductors in a mega watt field converter," *IEEE Transactions on Industrial Electronics*, pp. 1–1, 2019.

[12] U. M. Choi, F. Blaabjerg, and S. Jorgensen, "Junction temperature estimation for an advanced active power cycling test," in *2015 ICPE-ECCE Asia*, June 2015, pp. 2944–2950.

[13] P. Ghimire, I. Trintis, S. Munk-Nielsen, and B. Rannestad, "On-state voltage drop based derating/uprating on a mw converter to improve reliability," *Microel. Rel.*, vol. 58, pp. 90–94, 2016.

[14] P. Ghimire, K. B. Pedersen, I. Trintis, B. Rannestad, and S. Munk-Nielsen, "Online chip temperature monitoring using uce-load current and ir thermography," in *Proc. ECCE*, 2015, pp. 6602–6609.

[15] X. Perpiñà, J.-F. Serviere, J. Saiz, D. Barlini, M. Mermet-Guyennet, and J. Millán, "Temperature measurement on series resistance and devices in power packs based on on-state voltage drop monitoring at high current," *Microelectronics Reliability*, vol. 46, no. 9-11, pp. 1834–1839, 2006.

[16] Y.-S. Kim and S.-K. Sul, "On-line estimation of igbt junction temperature using on-state voltage drop," in *Industry Applications Conference, 1998. Thirty-Third IAS Annual Meeting. The 1998 IEEE*, vol. 2. IEEE, 1998, pp. 853–859.

[17] P. Ghimire, K. B. Pedersen, A. R. d. Vega, B. Rannestad, S. Munk-Nielsen, and P. B. Thogersen, "A real time measurement of junction temperature variation in high power igbt modules for wind power converter application," in *Integrated Power Systems (CIPS)*, 2014, pp. 1–6, iD: 1.

[18] S. Beczkowski, P. Ghimre, A. R. de Vega, S. Munk-Nielsen, B. Rannestad, and P. Thogersen, "Online vce measurement method for wear-out monitoring of high power igbt modules," in *Eur. Conf. Pow. El. and Appl. (EPE)*, Sept 2013, pp. 1–7.

[19] H. Kuhn and A. Mertens, "On-line junction temperature measurement of igbts based on temperature sensitive electrical parameters," in *2009 13th European Conference on Power Electronics and Applications*, Sept 2009, pp. 1–10.

[20] A. Bryant, S. Yang, P. Mawby, D. Xiang, L. Ran, P. Tavner, and P. R. Palmer, "Investigation into igbt dv/dt during turn-off and its temperature dependence," *IEEE Transactions on Power Electronics*, vol. 26, no. 10, pp. 3019–3031, 2011, iD: 1.

[21] D. W. Brown, M. Abbas, A. Ginart, I. N. Ali, P. W. Kalgren, and G. J. Vachtsevanos, "Turn-off time as an early indicator of insulated gate bipolar transistor latch-up," *IEEE Transactions on Power Electronics*, vol. 27, no. 2, pp. 479–489, 2012.

[22] Y. Yuan, D. Xiang, and C. Ning, "Self-calibration for igbt junction temperature measurement in power converter," in *2016 IEEE 8th International Power Electronics and Motion Control Conference (IPEMC-ECCE Asia)*, May 2016, pp. 3125–3130.

[23] H. Li, D. Xiang, X. Yang, and X. Zhang, "Compressed sensing method for igbt high-speed switching time on-line monitoring," *IEEE Transactions on Industrial Electronics*, pp. 1–1, 2018.

[24] S. Weber, M. Schluter, D. Borowski, and A. Mertens, "Simple analog detection of turn-off delay time for igbt junction temperature estimation," in *2016 IEEE Energy Conversion Congress and Exposition (ECCE)*, Sept 2016, pp. 1–7.

[25] X. Wang, C. Zhu, H. Luo, W. Li, and X. He, "Elimination of collector current impact in tsep-based junction temperature extraction method for high-power igbt modules," *Chinese Journal of Electrical Engineering*, vol. 2, no. 1, pp. 85–90, June 2016.

[26] D. Barlini, M. Ciappa, A. Castellazzi, M. Mermet-Guyennet, and W. Fichtner, "New technique for the measurement of the static and of the transient junction temperature in igbt devices under operating conditions," *Microelectronics Reliability*, vol. 46, no. 9-11, pp. 1772–1777, 2006.

[27] H. Luo, Y. Chen, W. Li, and X. He, "Online high-power p-i-n diode junction temperature extraction with reverse recovery fall storage charge," *IEEE Transactions on Power Electronics*, vol. 32, no. 4, pp. 2558–2567, April 2017.

[28] H. Luo, P. Sun, Y. Dong, W. Li, X. He, G. Chen, E. Yang, and Z. Dong, "P-i-n diode chip temperature extraction method by investigation into maximum recovery current rate di/dt," in *2014 IEEE Energy Conversion Congress and Exposition (ECCE)*, Sept 2014, pp. 4022–4024.

[29] N. Baker, S. Munk-Nielsen, F. Iannuzzo, and M. Liserre, "IGBT junction temperature measurement via peak gate current," *IEEE Transactions on Power Electronics*, vol. 31, no. 5, pp. 3784–3793, may 2016.

[30] M. Denk and M. M. Bakran, "Junction temperature measurement during inverter operation using a tj-igbt-driver," in *Proc. PCIM Europe*, 2015, pp. 1–8, iD: 1.

[31] B. Strauss and A. Lindemann, "Measuring the junction temperature of an IGBT using its threshold voltage as a temperature sensitive electrical parameter (TSEP)," in *2016 13th International Multi-Conference on Systems, Signals & Devices (SSD)*. IEEE, mar 2016.

[32] L. Dupont and Y. Avenas, "Preliminary evaluation of thermo-sensitive electrical parameters based on the forward voltage for online chip temperature measurements of IGBT devices," *IEEE Transactions on Industry Applications*, vol. 51, no. 6, pp. 4688–4698, nov 2015.

[33] C. J. M. Lasance, C. T. Murray, D. L. Saums, and M. Rencz, "Challenges in thermal interface material testing," in *Proc. IEEE Semicond. Therm. Meas. And Mng Symp.*, 2006, pp. 42–49.

[34] M. Ciappa, "Selected failure mechanisms of modern power modules," *Microelectronics reliability*, vol. 42, no. 4, pp. 653–667, 2002.

[35] B. Ji, X. Song, W. Cao, V. Pickert, Y. Hu, J. W. Mackersie, and G. Pierce, "In situdiagnostics and prognostics of solder fatigue in igbt modules for electric vehicle drives," *IEEE Transactions on Power Electronics*, vol. 30, no. 3, pp. 1535–1543, March 2015.

[36] C. E. Products and D. Center, "Design and process guidelines for use of ceramic chip capacitors," 16. March 2017. [Online]. Available: www.ieca-inc.com/images/Ceramic_capacitor_Failure_Mechanisms.pdf

[37] A. Wintrich, U. Nicolai, W. Tursky, and T. Reimann, *Application Manual Power Semiconductors*. Semikron International GmbH, 2011.

[38] N. McNeill, K. Sheng, B. W. Williams, and S. J. Finney, "Assessment of off-state negative gate voltage requirements for igbts," *IEEE Transactions on Power Electronics*, vol. 13, no. 3, pp. 436–440, 1998, iD: 1.

[39] S. Yang, D. Xiang, A. Bryant, P. Mawby, L. Ran, and P. Tavner, "Condition monitoring for device reliability in power electronic converters: A review," *IEEE Transactions on Power Electronics*, vol. 25, no. 11, pp. 2734–2752, 2010.

[40] B. Ji, V. Pickert, W. Cao, and B. Zahawi, "In situ diagnostics and prognostics of wire bonding faults in igbt modules for electric vehicle drives," *IEEE Transactions on Power Electronics*, vol. 28, no. 12, pp. 5568–5577, 2013, iD: 1.

[41] R. O. Nielsen, J. Due, and S. Munk-Nielsen, "Innovative measuring system for wear-out indication of high power igbt modules," in *Proc. ECCE*, 2011, pp. 1785–1790.

[42] P. Ghimire, A. R. de Vega, S. Beczkowski, B. Rannestad, S. Munk-Nielsen, and P. Thogersen, "Improving power converter reliability: Online monitoring of high-power igbt modules," *IEEE Ind. El. Mag.*, vol. 8, no. 3, pp. 40–50, 2014.

[43] P. Ghimire, "Real time monitoring and wear out of power modules," Ph.D. dissertation, 2015.

[44] U.-M. Choi, F. Blaabjerg, S. Jorgensen, S. Munk-Nielsen, and B. Rannestad, "Reliability improvement of power converters by means of condition monitoring of IGBT modules," *IEEE Trans. Pow. El.*, vol. 32, no. 10, pp. 7990–7997, oct 2017.

[45] T. Krone, L. D. Hung, M. Jung, and A. Mertens, "Advanced condition monitoring system based on on-line semiconductor loss measurements," in *2016 IEEE Energy Conversion Congress and Exposition (ECCE)*, Sept 2016, pp. 1–8.

[46] W. L. Gans, "The measurement and deconvolution of time jitter in equivalent-time waveform samplers," *IEEE Transactions on Instrumentation and Measurement*, vol. 32, no. 1, pp. 126–133, 1983.

[47] M. O. Sonnaillon, R. Urteaga, and F. J. Bonetto, "High-frequency digital lock-in amplifier using random sampling," *IEEE Transactions on Instrumentation and Measurement*, vol. 57, no. 3, pp. 616–621, March 2008.

[48] P. D. Hale, C. M. Wang, D. F. Williams, K. A. Remley, and J. D. Wepman, "Compensation of random and systematic timing errors in sampling oscilloscopes," *IEEE Transactions on Instrumentation and Measurement*, vol. 55, no. 6, pp. 2146–2154, Dec 2006.

[49] S. J. Liu, P. P. Qi, J. S. Wang, M. H. Zhang, and W. S. Jiang, "Adaptive calibration of channel mismatches in time-interleaved adcs based on equivalent signal recombination," *IEEE Transactions on Instrumentation and Measurement*, vol. 63, no. 2, pp. 277–286, Feb 2014.

[50] Y. Zhao, Y. H. Hu, and H. Wang, "Enhanced random equivalent sampling based on compressed sensing," *IEEE Transactions on Instrumentation and Measurement*, vol. 61, no. 3, pp. 579–586, March 2012.

[51] A. Agoston, "Equivalent time pseudorandom sampling system," Jul. 7 1987, uS Patent 4,678,345.

[52] W. MacDonald, M. J. Woodward, and S. W. Hinch, "Internally triggered equivalent-time sampling system for signals having a predetermined data rate," Jan. 30 2001, uS Patent 6,181,267.

[53] P. J. Pupalaikis and LeCroy, "Random interleaved sampling (ris)." [Online]. Available: http://cdn.teledynelecroy.com/files/whitepapers/wp_ris_102203.pdf

[54] Tektronix, "Technique primer 47w-7209. sampling oscilloscope techniques." [Online]. Available: https://www.tek.com/sites/default/files/media/media/resources/Sampling%20Oscilloscope%20Techniques.pdf

[55] Keysight technologies, "Application note. what is the difference between an equivalent time sampling oscilloscope and a real-time oscilloscope?" [Online]. Available: http://literature.cdn.keysight.com/litweb/pdf/5989-8794EN.pdf

[56] E. J. Candes and M. B. Wakin, "An introduction to compressive sampling," *IEEE Signal Processing Magazine*, vol. 25, no. 2, pp. 21–30, March 2008.

[57] J. Ma, "Compressed sensing for surface characterization and metrology," *IEEE Transactions on Instrumentation and Measurement*, vol. 59, no. 6, pp. 1600–1615, June 2010.

[58] D. Schneider, "New camera chip captures only what it needs," *IEEE Spectrum*, vol. 50, no. 3, pp. 13–14, March 2013.

[59] M. Lustig, D. Donoho, and J. M. Pauly, "Sparse mri: The application of compressed sensing for rapid mr imaging," *Magnetic Resonance in Medicine: An Official Journal of the International Society for Magnetic Resonance in Medicine*, vol. 58, no. 6, pp. 1182–1195, 2007.

[60] J. Bobin, J. Starck, and R. Ottensamer, "Compressed sensing in astronomy," *IEEE Journal of Selected Topics in Signal Processing*, vol. 2, no. 5, pp. 718–726, Oct 2008.

[61] S. Barla, "Wood mckenzie global wind turbine technology database," Tech. Rep.

[62] F. Blaabjerg, M. Liserre, and K. Ma, "Power electronics converters for wind turbine systems," *IEEE Transactions on Industry Applications*, vol. 48, no. 2, pp. 708–719, 2012.

[63] B. S. Everitt, Ed., *Cambridge Dictionary of Statistics, 2nd ed.*, 2002, p. 360.

Christian Uhrenfeldt received his M.Sc. in Physics from Aalborg University in 2004. In 2008 he received the Ph.D. degree in the field of semiconductor material science from Aarhus University.

He is currently working as Associate professor at the Department of Energy Technology at Aalborg University on power electronics packaging and materials. His research interests include packaging of power modules, nondestructive testing and semiconductor diagnostics in power electronics.

Bjørn Rannestad received the M.Sc. and PhD degrees in electrical engineering from Aalborg University, Aalborg, Denmark, in 1999 and 2019, respectively. He is currently working as a senior specialist in converters at KK Wind Solutions, Ikast, Denmark. From 1999 to 2008, he was with Grundfos, Bjerringbro, Denmark, where he led the hardware design of several products of electronic controlled pumps, including the power electronic design platform for future products. Since 2008, he has been with KK Wind Solutions, Ikast, Denmark, working with high-power converters for wind turbines. He has been focusing on improving the robustness and reliability of power converters by means of condition monitoring. Lately, he has initiated a field test project of a converter monitoring unit for wind turbine converters. The field test project was an enabler for his industrial PhD project. His research interests include reliability of power devices, power electronic converters and renewable power generation.

Stig Munk-Nielsen received the M.Sc. and PhD degrees in electrical engineering from Aalborg University, Aalborg, Denmark, in 1991 and 1997, respectively. He is currently Professor WSR at the Department of Energy Technology, Aalborg University. His research interests Include LV and MV converters, packaging of power electronic devices, electrical monitoring apparatus for devices, failure modes and device test systems. In the last ten years, he has been involved or has managed 10 research projects, including national and European Commission projects.

Kristian Gadgaard received the B.Sc in Electrical Engineering from Aarhus University, Denmark, in 1986. He is currently manager at Phillips Medisize, Struer, Denmark. From 1986 to 1988, he was with Storno as a development engineer on cell phones. From 1988 to 1995 and 2010 to 2011, he was with Bang & Olufsen as development engineer, product coordinator and purchasing manager on audio products and radio frequency technologies. From 1996 to 2010 he was with Ericsson, Denmark, as system engineer and HW manager on optical interface and power supply systems for telecommunication. From 2010 to 2018 he was with KK Wind Solutions, Ikast, Denmark as project and hardware manager.